














The Open Cluster Chemical Abundances and Mapping Survey. IV. Abundances for 128 Open Clusters Using SDSS/APOGEE DR16

Item Type	Article
Authors	Donor, John; Frinchaboy, Peter M.; Cunha, Katia; O'Connell, Julia E.; Prieto, Carlos Allende; Almeida, Andrés; Anders, Friedrich; Beaton, Rachael; Bizyaev, Dmitry; Brownstein, Joel R.; Carrera, Ricardo; Chiappini, Cristina; Cohen, Roger; García-Hernández, D. A.; Geisler, Doug; Hasselquist, Sten; Jönsson, Henrik; Lane, Richard R.; Majewski, Steven R.; Minniti, Dante; Bidin, Christian Moni; Pan, Kaike; Roman-Lopes, Alexandre; Sobeck, Jennifer S.; Zasowski, Gail
Citation	John Donor et al 2020 AJ 159 199
DOI	10.3847/1538-3881/ab77bc
Publisher	IOP PUBLISHING LTD
Journal	ASTRONOMICAL JOURNAL
Rights	© 2020. The American Astronomical Society. All rights reserved.
Download date	27/08/2022 20:19:14
Item License	http://rightsstatements.org/vocab/InC/1.0/
Version	Final published version
Link to Item	http://hdl.handle.net/10150/641216



The Open Cluster Chemical Abundances and Mapping Survey. IV. Abundances for 128 Open Clusters Using SDSS/APOGEE DR16

John Donor¹, Peter M. Frinchaboy¹ , Katia Cunha^{2,3} , Julia E. O’Connell⁴, Carlos Allende Prieto^{5,6}, Andrés Almeida⁷, Friedrich Anders⁸, Rachael Beaton^{9,10,29,30} , Dmitry Bizyaev^{11,12} , Joel R. Brownstein¹³ , Ricardo Carrera¹⁴ , Cristina Chiappini¹⁵, Roger Cohen¹⁶, D. A. García-Hernández^{5,6}, Doug Geisler^{4,7,17} , Sten Hasselquist^{13,31}, Henrik Jönsson^{18,19}, Richard R. Lane^{20,21}, Steven R. Majewski²², Dante Minniti^{23,24,25} , Christian Moni Bidin²⁶, Kaike Pan¹¹ , Alexandre Roman-Lopes²⁷ , Jennifer S. Sobeck²⁸, and Gail Zasowski¹³ 

¹ Department of Physics & Astronomy, Texas Christian University, TCU Box 298840, Fort Worth, TX 76129, USA; j.donor@tcu.edu, p.frinchaboy@tcu.edu

² Steward Observatory, The University of Arizona, 933 North Cherry Avenue, Tucson, AZ 85721-0065, USA

³ Observatório Nacional, Rua General José Cristino, 77, 20921-400 São Cristóvão, Rio de Janeiro, RJ, Brazil

⁴ Departamento de Astronomía, Universidad de Concepción, Casilla 160-C, Concepción, Chile

⁵ Instituto de Astrofísica de Canarias, Vía Láctea S/N, E-38205 La Laguna, Tenerife, Spain

⁶ Universidad de La Laguna, Departamento de Astrofísica, E-30206 La Laguna, Tenerife, Spain

⁷ Instituto de Investigación Multidisciplinario en Ciencia y Tecnología, Universidad de La Serena, Benavente 980, La Serena, Chile

⁸ Departament de Física Quàntica i Astrofísica, Universitat de Barcelona, IEEC-UB, Martí i Franquès 1 E-08028 Barcelona, Spain

⁹ Department of Astrophysical Sciences, Princeton University, 4 Ivy Lane, Princeton, NJ 08544, USA

¹⁰ The Observatories of the Carnegie Institution for Science, 813 Santa Barbara St., Pasadena, CA 91101, USA

¹¹ Apache Point Observatory and New Mexico State University, P.O. Box 59, sunspot, NM, 88349-0059, USA

¹² Sternberg Astronomical Institute, Moscow State University, Moscow, Russia

¹³ Department of Physics & Astronomy, University of Utah, 115 S. 1400 E., Salt Lake City, UT 84112, USA

¹⁴ Astronomical Observatory of Padova, National Institute of Astrophysics, Vicolo Osservatorio 5-35122—Padova, Italy

¹⁵ Leibniz-Institut für Astrophysik Potsdam (AIP), An der Sternwarte 16, D-14482 Potsdam, Germany

¹⁶ Space Telescope Science Institute, 3700 San Martin Drive, Baltimore, MD 21218, USA

¹⁷ Departamento de Astronomía, Universidad de La Serena, Avenida Juan Cisternas 1200, La Serena, Chile

¹⁸ Materials Science and Applied Mathematics, Malmö University, SE-205 06 Malmö, Sweden

¹⁹ Lund Observatory, Department of Astronomy and Theoretical Physics, Lund University, Box 43, SE-22100 Lund, Sweden

²⁰ Instituto de Astrofísica, Pontificia Universidad Católica de Chile, Av. Vicuña Mackenna 4860, 782-0436 Macul, Santiago, Chile

²¹ Instituto de Astronomía y Ciencias Planetarias, Universidad de Atacama, Copayapu 485, Copiapó, Chile

²² Department of Astronomy, University of Virginia, Charlottesville, VA 22904-4325, USA

²³ Departamento de Ciencias Físicas, Facultad de Ciencias Exactas, Universidad Andres Bello, Av. Fernandez Concha 700, Las Condes, Santiago, Chile

²⁴ Millennium Institute of Astrophysics, Av. Vicuña Mackenna 4860, 782-0436, Santiago, Chile

²⁵ Vatican Observatory, V00120 Vatican City State, Italy

²⁶ Instituto de Astronomía, Universidad Católica del Norte, Av. Angamos 0610, Antofagasta, Chile

²⁷ Department of Astronomy—Universidad de La Serena—Av. Juan Cisternas, 1200 North, La Serena, Chile

²⁸ Department of Astronomy, University of Washington, Seattle, WA, 98195, USA

Received 2019 December 9; revised 2020 February 14; accepted 2020 February 17; published 2020 April 10

Abstract

The Open Cluster Chemical Abundances and Mapping (OCCAM) survey aims to constrain key Galactic dynamical and chemical evolution parameters by the construction of a large, comprehensive, uniform, infrared-based spectroscopic data set of hundreds of open clusters. This fourth contribution from the OCCAM survey presents analysis using Sloan Digital Sky Survey/APOGEE DR16 of a sample of 128 open clusters, 71 of which we designate to be “high quality” based on the appearance of their color–magnitude diagram. We find the APOGEE DR16 derived [Fe/H] abundances to be in good agreement with previous high-resolution spectroscopic open cluster abundance studies. Using the high-quality sample, we measure Galactic abundance gradients in 16 elements, and find evolution of some of the [X/Fe] gradients as a function of age. We find an overall Galactic [Fe/H] versus R_{GC} gradient of -0.068 ± 0.001 dex kpc⁻¹ over the range of $6 < R_{GC} < 13.9$ kpc; however, we note that this result is sensitive to the distance catalog used, varying as much as 15%. We formally derive the location of a break in the [Fe/H] abundance gradient as a free parameter in the gradient fit for the first time. We also measure significant Galactic gradients in O, Mg, S, Ca, Mn, Cr, Cu, Na, Al, and K, some of which are measured for the first time. Our large sample allows us to examine four well-populated age bins in order to explore the time evolution of gradients for a large number of elements and comment on possible implications for Galactic chemical evolution and radial migration.

Unified Astronomy Thesaurus concepts: Open star clusters (1160); Galactic abundances (2002); Milky Way evolution (1052); Chemical abundances (224)

Supporting material: machine-readable tables

1. Introduction

In this era of multifiber spectrographs, studies of tens of thousands of stars across the Galaxy are common. However, to derive critical parameters such as age and distance, the importance of reliable calibration samples cannot be understated. Open clusters

²⁹ Hubble Fellow.

³⁰ Carnegie-Princeton Fellow.

³¹ NSF Astronomy and Astrophysics Fellow.

serve as reliable age, distance, and chemical tracers distributed around the Galactic disk.

Open clusters have been used to study Galactic chemical trends as far back as Janes (1979), where the author showed open clusters to be a reliable tracer of a Galactic radial metallicity gradient. More recently, this trend has been consistently considered a two-function gradient (e.g., Bragaglia et al. 2008; Sestito et al. 2008; Friel et al. 2010; Carrera & Pancino 2011; Yong et al. 2012; Frinchaboy et al. 2013; Reddy et al. 2016; Magrini et al. 2017), with the break falling between $R_{GC} \approx 10$ kpc and $R_{GC} \approx 16$ kpc. This gradient has become an important observable constraint for models of Galactic Chemical Evolution. Recent work has measured the inner gradient to be between -0.05 dex kpc^{-1} (Reddy et al. 2016; Casamiquela et al. 2019) and -0.1 dex kpc^{-1} (Jacobson et al. 2016). In addition, Donor et al. (2018) (henceforth OCCAMII) showed that this gradient could change by as much as 40%, depending on which distance catalog was used.

Because open clusters can range in age from a few Myr to more than 6 Gyr, they also provide a unique opportunity to study the evolution of Galactic abundance gradients. A number of authors have measured metallicity gradients for open clusters in various age bins (e.g., Carraro et al. 1998; Friel et al. 2002; Carrera & Pancino 2011; Jacobson et al. 2011; Cunha et al. 2016), and while all studies agree that the gradient is shallower for younger clusters, further comparison is difficult due to a somewhat heterogeneous choice of age bins; there does not seem to be a consensus as to the measured gradient for clusters of any given age range.

Indeed, there are indications the picture is even more complicated. While open clusters have the advantage of precise age estimates, there are complexities that must be considered when using them to probe Galactic evolution. Anders et al. (2017) suggest that open clusters in the inner galaxy are more likely to be broken up, leading to samples significantly biased toward younger clusters.

Galactic trends in elements besides iron have been reported (e.g., Yong et al. 2005; Friel et al. 2010; Jacobson et al. 2011). Trend lines are commonly fit for α -elements (e.g., Carrera & Pancino 2011; Yong et al. 2012; Reddy et al. 2016), and in some cases for other elements, such as $[\text{Ni}/\text{Fe}]$, $[\text{Cr}/\text{Fe}]$, and $[\text{V}/\text{Fe}]$ (Casamiquela et al. 2019) or $[\text{Na}/\text{Fe}]$ and $[\text{Al}/\text{Fe}]$ (Yong et al. 2012). There is a growing consensus that there is a mild positive $[\alpha/\text{Fe}]$ versus R_{GC} trend in the inner galaxy, similar to some chemodynamical model predictions (see Minchev et al. 2014). OCCAMII showed the value of studying trends in other elements, finding strong evidence for a negative trend in $[\text{Mn}/\text{Fe}]$ versus R_{GC} .

In this paper, we will present the expanded OCCAM sample based on results from Sloan Digital Sky Survey (SDSS) IV Apache Point Observatory Galactic Evolution Experiment 2 (APOGEE 2; Majewski et al. 2017) Data Release 16 (DR16) (H. Jönsson et al. 2020, in preparation). We discuss this sample in comparison to the previously studied sample of open clusters that used SDSS IV DR14 results (OCCAMII), as well as other results from the literature. We then explore Galactic trends in $[\text{Fe}/\text{H}]$, α elements, iron-peak elements, and all other elements reported by APOGEE as a function of Galactocentric distances. We finally break the sample into age bins to explore changes in radial abundance trends over time.

2. Data

To minimize the impact of calibration differences and other systematic effects, and ensure uniformity, the OCCAM survey uses as much data from as few sources as possible. Therefore, the majority of this analysis is based primarily on two large surveys: *Gaia* and SDSS/APOGEE.

Our primary source of chemical abundance and radial velocity (RV) data is the SDSS sixteenth data release (DR16; Ahumada et al. 2019; H. Jönsson et al. 2020, in preparation; Blanton et al. 2017) taken as part of the second, dual-hemisphere phase of APOGEE (APOGEE 2; Majewski et al. 2017). APOGEE is a high-resolution, near-infrared spectroscopic survey currently operating in both hemispheres, at APO (New Mexico, Gunn et al. 2006) and Las Campanas Observatory (LCO; Chile, Bowen, & Vaughan 1973). The APOGEE/DR16 data set includes about 430,000 stars, collected between 2011 August and 2018 August using the two 300-fiber APOGEE spectrographs (Wilson et al. 2019), and for the first time, the APOGEE survey has near-complete coverage in Galactic longitude, due to the first release of data from LCO. The APOGEE data reduction pipeline (Nidever et al. 2015; Holtzman et al. 2015, 2018, H. Jönsson et al. 2020, in preparation) provides stellar atmospheric parameters and radial velocity measurements, while elemental abundances are provided from the ASPCAP pipeline (García Pérez et al. 2016; Mészáros et al. 2012; Zamora et al. 2015; Holtzman et al. 2018, H. Jönsson et al. 2020, in preparation). Copper, cerium (Cunha et al. 2017), neodymium (Hasselquist et al. 2016), and ytterbium abundances are reported from ASPCAP for the first time in DR16, although neodymium and ytterbium lines are so weak or blended that these ASPCAP abundances are considered unreliable. Concerning cerium, the APOGEE region contains several Ce II lines (Cunha et al. 2017). However, the current DR16 results are only based on one Ce II line; future data releases will use the full sample of cerium lines. Therefore, we will postpone any discussion of cerium until future data releases.

In the APOGEE DR16 allStar-file, several types of abundances are reported for every star and element. First, the abundance reported by the analysis pipeline is supplied in the FELEM-array. Second, these abundances have been calibrated with a zero-point shift to ensure solar metallicity stars in the solar neighborhood have $[X/M] = 0$; in practice, these shifts are small, <0.05 dex, except for Al, K, V, and Mn. Finally, these calibrated abundances have been culled for particular uncertain values by the ASPCAP-team (e.g., for $[\text{Y}/\text{Fe}]$ or $[\text{Nd}/\text{Fe}]$). These final “cleaned” and calibrated abundances are supplied in the “named tags:” FE_H, MG_FE, CE_FE, etc. More information, including what zero-point shifts have been applied, is provided in H. Jönsson et al. (2020, in preparation). In this paper, we use the abundances of the “named tags” as is recommended in H. Jönsson et al. (2020, in preparation).

Targeting for APOGEE relied on input from two all-sky surveys: 2MASS (Skrutskie et al. 2006) and the *Wide-field Infrared Survey Explorer* (Wright et al. 2010). More details specifically about open cluster targeting are provided in OCCAMII, and details about APOGEE targeting generally can be found in Zasowski et al. (2013, 2017).

Our secondary source of data is *Gaia* DR2 (Gaia Collaboration et al. 2016, 2018; Lindegren et al. 2018); we use photometric and astrometric data for 1,365,376 *Gaia* stars,

DONOR ET AL.

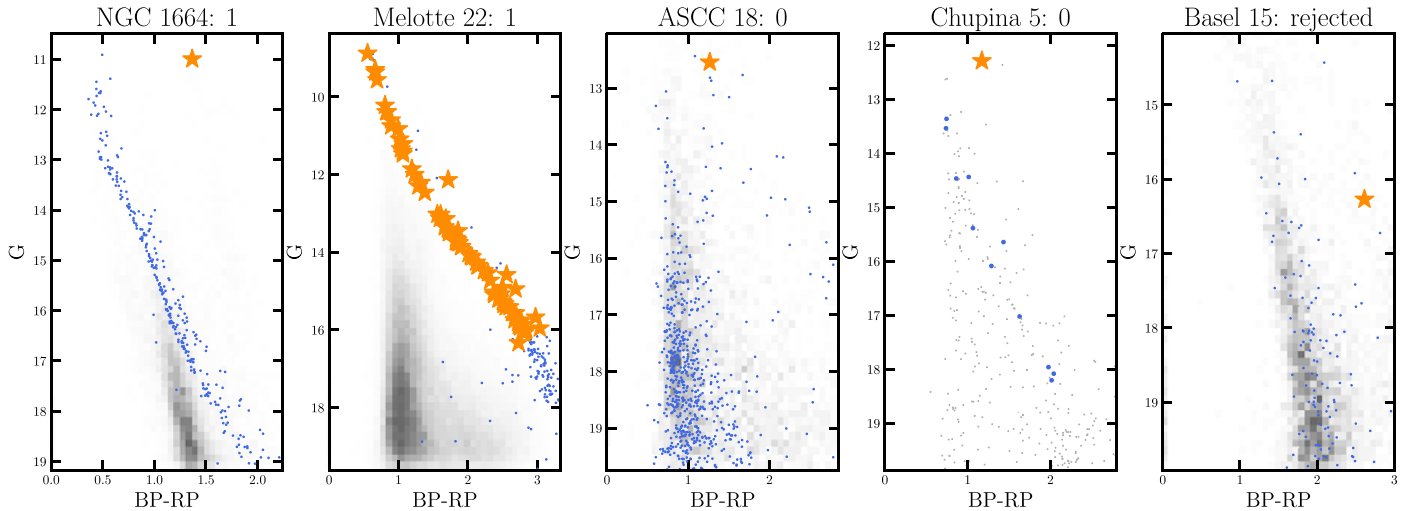


Figure 1. Five example color–magnitude diagrams of open clusters analyzed in the study, with cluster name and quality designation from Table 1. *Gaia* stars within twice the cluster radius are shown; stars identified as PM members and inside the cluster radius are blue. Nonmember stars are shown as a Hess diagram in gray except for Chupina 5, where actual stars are shown. The OCCAM pipeline-identified APOGEE members are shown as orange stars.

radial velocity measurements for 16,084 stars, and parallax values for 886 stars in common with APOGEE.

We use cluster coordinates and radii from Dias et al. (2002). For this study, we use the uniform distance determination from Kharchenko et al. (2013), which is generally referred to as the Milky Way Star Cluster (MWSC) catalog when measuring galactic trends; however, we briefly compare to other uniform distance catalogs (e.g., Bailer-Jones et al. 2018; Cantat-Gaudin et al. 2018) in Section 5.1.

3. Methods

3.1. Membership Analysis

The selection of cluster member stars utilizes the stellar radial velocities, proper motions (PM), spatial location, and derived metallicities as membership discriminators. For this study, we use the membership procedure, fully described in OCCAMII with some minor improvements. The method of OCCAMII first performs a PM analysis using *Gaia* DR2 to isolate likely cluster members. If multiple APOGEE stars are selected for the same cluster that have very different RVs, there is an inherent ambiguity and a “correct” systemic cluster velocity cannot be chosen. We now leverage the RV measurements from *Gaia*, when available, for stars identified as likely PM members to significantly increase the number of RV measurements in a cluster and more reliably determine the cluster system velocity.

To be included as a cluster member, a star must fall within 3σ of the cluster mean as established by the kernel convolution (described in OCCAMII) in *all three* spaces considered (RV, [Fe/H], and PM).

3.2. Visual Quality Check

A visual inspection of each cluster’s PM-cleaned color–magnitude diagram (CMD) was performed by several of the authors. Figure 1 shows five example CMDs. The visual assessment is meant to evaluate whether stars that pass the combined RV, proper motion and metallicity criteria also lie in a sensible position in the observed cluster CMD, considering

their spectroscopically determined $\log(g)$. This is an easy case when, for example, one or more APOGEE OCCAM candidates with high $\log(g)$ ($\log(g) \geq 3.7$) are found to lie along an easily discernible photometric main sequence in the CMD (e.g., Melotte 22), thus providing a joint affirmation that the star is likely a main-sequence member of the cluster. These clusters are flagged as “1” or “high quality.” However, most of the OCCAM stars from APOGEE turn out to be evolved stars—subgiants, giants and red clump stars, with $\log(g) < 3.7$. In this case, the star is still considered a member if the star lies along the subgiant/giant branch of the cluster—which, however, must generally be projected from the location of the main sequence and its turn-off, given that the subgiant/giant sequences in most clusters are typically very poorly populated (e.g., NGC 1664). These clusters are also flagged as “1” or “high quality.” The latter process becomes more challenging when the main sequence is also poorly populated (e.g., Chupina 5), or when the field star contamination becomes so dominant as to obscure the cluster main sequence (e.g., ASCC 18). These clusters are flagged as “0” or “potentially unreliable.” Clusters where the APOGEE OCCAM candidate is not a part of any discernible sequence or where there is no discernible sequence (e.g., Basel 15) are rejected. These quality flags are included in the full version of Tables 1 and 2 (available online), as well as in the value-added catalog, described below.

3.3. Data Access—SDSS Value-added Catalog

The data this analysis uses are also available as a value-added catalog (VAC) that was released along with SDSS-IV DR16. The VAC consists of two tables. The first is a combination of Tables 1 and 2, showing bulk cluster parameters derived here including PM and RV, but also including abundances for all³² elements reported in DR16. We note that cluster ages are not included in the VAC, as only ages from the MWSC catalog are used in this work.

³² Elements such as Rb and Y that do not have calibrated values reported in DR16 are not included.

Table 1
OCCAM DR16 Sample—Basic Parameters

Cluster name	Qual flag	l deg	b deg	R^a (′)	Age ^b Gyr	R_{GC}^b (kpc)	μ_α^c (mas yr ⁻¹)	μ_δ^c (mas yr ⁻¹)	RV (km s ⁻¹)	[Fe/H] (dex)	Num stars
High-quality Clusters											
Ruprecht 147	1	21.0089	-12.7301	30.0	2.14	7.72	-0.87 ± 0.10	-26.72 ± 0.10	+42.4 ± 1.5	+0.12 ± 0.03	27
NGC 6705	1	27.2873	-2.7594	9.0	0.32	5.94	-1.56 ± 0.08	-4.17 ± 0.07	+35.4 ± 1.0	+0.12 ± 0.04	12
Berkeley 43	1	45.6843	-0.1391	6.3	0.61	5.73	-0.92 ± 0.08	-3.27 ± 0.07	+30.0 ± 0.1	+0.03 ± 0.01	1
Berkeley 44	1	53.2093	+3.3443	6.3	1.41	6.50	-0.17 ± 0.05	-3.17 ± 0.05	+23.0 ± 0.1	-0.00 ± 0.01	1
NGC 6791	2	69.9658	+10.9080	6.3	4.42	7.71	-0.44 ± 0.03	-2.25 ± 0.03	-46.9 ± 1.3	+0.35 ± 0.04	36
NGC 6819	2	73.9834	+8.4882	6.9	1.62	7.70	-2.96 ± 0.03	-3.87 ± 0.03	+2.7 ± 1.7	+0.05 ± 0.03	37
NGC 6811	2	79.2233	+12.0047	7.2	0.64	7.87	-3.44 ± 0.06	-8.73 ± 0.04	+8.0 ± 0.3	-0.05 ± 0.02	4
NGC 6866	1	79.5648	+6.8354	5.1	0.44	7.87	-1.18 ± 0.04	-5.91 ± 0.08	+14.2 ± 0.4	+0.01 ± 0.01	2
IC 1369	1	89.6019	-0.4154	5.1	0.35	8.70	-4.68 ± 0.05	-5.55 ± 0.04	-48.5 ± 0.1	-0.08 ± 0.03	3
NGC 7062	1	89.9667	-2.7397	3.6	0.69	8.34	-1.84 ± 0.04	-4.08 ± 0.04	-22.0 ± 0.1	+0.01 ± 0.01	1
.....											

Notes.^a Radius from Dias et al. (2002).^b Calculated using or taken from MWSC Catalog.^c Here, μ_α and μ_δ and their 1σ uncertainties are those of the 2D Gaussian fit, as in OCCAMII.

(This table is available in its entirety in machine-readable form.)

Table 2
OCCAM DR16 Sample—Detailed Chemistry

Cluster name	[Fe/H] (dex)	[O/Fe] (dex)	[Na/Fe] (dex)	[Mg/Fe] (dex)	[Al/Fe] (dex)	[Si/Fe] (dex)	[S/Fe] (dex)	[K/Fe] (dex)
	[Ca/Fe] (dex)	[Ti/Fe] (dex)	[V/Fe] (dex)	[Cr/Fe] (dex)	[Mn/Fe] (dex)	[Co/Fe] (dex)	[Ni/Fe] (dex)	[Cu/Fe] (dex)
High-quality Clusters								
Ruprecht 147	0.12 ± 0.03	-0.05 ± 0.03	0.11 ± 0.03	-0.01 ± 0.02	0.02 ± 0.04	-0.00 ± 0.05	0.02 ± 0.06	0.04 ± 0.08
	-0.01 ± 0.04	-0.07 ± 0.09	0.01 ± 0.07	0.02 ± 0.09	0.04 ± 0.03	0.14 ± 0.20	0.01 ± 0.02	-0.09 ± 0.20
NGC 6705	0.12 ± 0.04	-0.05 ± 0.02	0.23 ± 0.04	-0.07 ± 0.02	-0.13 ± 0.03	0.01 ± 0.01	0.07 ± 0.02	-0.16 ± 0.06
	-0.03 ± 0.02	-0.00 ± 0.02	-0.01 ± 0.04	-0.03 ± 0.04	0.11 ± 0.02	0.04 ± 0.03	0.03 ± 0.01	0.17 ± 0.07
Berkeley 43	0.03 ± 0.01	-0.05 ± 0.01	0.15 ± 0.03	-0.08 ± 0.01	-0.22 ± 0.02	0.03 ± 0.01	0.13 ± 0.02	-0.18 ± 0.03
	-0.05 ± 0.01	-0.01 ± 0.01	-0.02 ± 0.04	-0.08 ± 0.03	0.12 ± 0.01	0.01 ± 0.03	0.02 ± 0.01	-0.26 ± 0.03
Berkeley 44	-0.00 ± 0.01	0.04 ± 0.01	-0.16 ± 0.03	-0.02 ± 0.01	-0.30 ± 0.02	0.01 ± 0.01	0.02 ± 0.03	-0.15 ± 0.03
	-0.14 ± 0.01	-0.13 ± 0.01	-0.29 ± 0.04	-0.17 ± 0.03	0.06 ± 0.01	0.05 ± 0.03	-0.03 ± 0.01	0.04 ± 0.03
NGC 6791	0.35 ± 0.04	0.04 ± 0.03	0.08 ± 0.06	0.11 ± 0.03	0.01 ± 0.07	0.01 ± 0.03	-0.02 ± 0.05	0.03 ± 0.10
	-0.02 ± 0.03	0.09 ± 0.05	-0.06 ± 0.30	-0.02 ± 0.09	0.01 ± 0.13	0.11 ± 0.08	0.01 ± 0.04	0.14 ± 0.07
NGC 6819	0.05 ± 0.03	-0.01 ± 0.03	0.07 ± 0.09	-0.01 ± 0.01	-0.04 ± 0.03	0.00 ± 0.03	0.00 ± 0.03	-0.04 ± 0.07
	0.01 ± 0.02	0.01 ± 0.03	0.04 ± 0.13	0.01 ± 0.03	0.05 ± 0.03	0.02 ± 0.06	0.02 ± 0.02	0.04 ± 0.06
NGC 6811	-0.05 ± 0.02	-0.04 ± 0.02	0.06 ± 0.07	-0.04 ± 0.01	-0.07 ± 0.03	-0.02 ± 0.01	0.05 ± 0.04	-0.06 ± 0.05
	0.02 ± 0.01	0.00 ± 0.02	...	0.05 ± 0.03	0.01 ± 0.02	-0.16 ± 0.12	-0.03 ± 0.01	-0.06 ± 0.10
NGC 6866	0.01 ± 0.01	...	-0.00 ± 0.04	-0.05 ± 0.01	-0.04 ± 0.02	-0.04 ± 0.01	0.04 ± 0.03	-0.06 ± 0.03
	0.01 ± 0.02	0.01 ± 0.02	...	0.03 ± 0.05	0.02 ± 0.01	-0.14 ± 0.08	-0.03 ± 0.01	0.02 ± 0.03
IC 1369	-0.08 ± 0.03	-0.08 ± 0.02	0.08 ± 0.10	-0.04 ± 0.02	-0.11 ± 0.02	-0.01 ± 0.01	0.09 ± 0.07	0.02 ± 0.03
	0.01 ± 0.04	-0.08 ± 0.02	...	0.01 ± 0.04	0.04 ± 0.03	-0.04 ± 0.04	-0.06 ± 0.01	0.09 ± 0.04
NGC 7062	0.01 ± 0.01	...	0.17 ± 0.04	-0.07 ± 0.01	-0.05 ± 0.02	-0.01 ± 0.01	0.00 ± 0.03	-0.05 ± 0.03
	-0.00 ± 0.01	-0.02 ± 0.02	...	-0.08 ± 0.03	-0.00 ± 0.01	0.01 ± 0.04	-0.02 ± 0.01	-0.04 ± 0.03
.....								

(This table is available in its entirety in machine-readable form.)

Five measurements of R_{GC} are also included. We calculate R_{GC} using catalog distances from Dias et al. (2002),³³ Kharchenko et al. (2013, MWSC), and Cantat-Gaudin et al. (2018). We also calculate R_{GC} based on median parallax from

member stars and median distance for member stars from Bailer-Jones et al. (2018), as in OCCAMII. In Section 5.1, we discuss differences in these distance measurements.

The second table in the VAC shows all of the APOGEE stars considered in this analysis (all the stars that fall within $2 \times R_{Dias}$ of the cluster center). For each star, we reproduce relevant parameters (RV, [Fe/H], and proper motion) and provide our membership probability estimate based on each parameter. For convenience, we also provide the

³³ We acknowledge an error in our pipeline that populated R_{GC} for some clusters where no distance is reported by Dias et al. (2002). “R_GC_DIAS” values for the clusters ASCC 16, Chupina 3, 4, and 5, Collinder 95, FSR 0687, L 1241 s, NGC 358, and Platais 4 should be disregarded.

Table 3

A Summary of the Individual Star Data Included in the DR16 OCCAM VAC

Label	Description
CLUSTER	The associated open cluster
2MASS ID	star ID from 2MASS survey
LOCATION_ID ^a	from APOGEE DR16
GLAT	Galactic latitude
GLON	Galactic longitude
FE_H ^a	[Fe/H]
FE_H_ERR ^a	uncertainty in FE_H
VHELIO_AVG ^a	heliocentric radial velocity
VSCATTER ^a	scatter in APOGEE RV measurements
PMRA ^b	proper motion in R.A.
PMDEC ^b	proper motion in decl.
PMRA_ERR ^b	uncertainty in PMRA
PMDEC_ERR ^b	uncertainty in PMDEC
RV_PROB	membership probability based on RV (This study)
FEH_PROB	membership probability based on FE_H (This study)
PM_PROB	membership probability based on PM (This study)
CG_PROB	membership probability from Cantat-Gaudin et al. (2018)

Notes.^a Taken directly from APOGEE DR16.^b From *Gaia* DR2.

membership determination from Cantat-Gaudin et al. (2018) (when provided). All columns available in the VAC are presented in Table 3. The catalog is available from sdss.org here.³⁴

Both tables are also available for exploration using Filtergraph (Burger et al. 2013) at https://filtergraph.com/sdss_apogee_occam/.

4. The OCCAM DR16 Sample

Our final sample in this study consists of 128 open clusters with 914 member stars, out of 10,191 stars near cluster fields considered in the analysis. Of those 128 clusters, 83 clusters were designated as “high quality” based on a visual CMD inspection. For the Galactic abundance analysis in this study, we will only use those clusters flagged as high quality, as presented in Table 1. The other clusters with questionable quality, e.g., those that did not pass visual checks (Section 3.2), are also presented in Table 1.

The Galactic spatial distribution of the OCCAM DR16 sample is shown in Figure 2. The majority of the OCCAM DR16 open clusters fall between $6 \leq R_{GC} \leq 14$ kpc, with good R_{GC} coverage in that range. Two high-quality clusters fall outside of this range: Berkeley 20 at $R_{GC} \approx 15.5$ kpc and Berkeley 29 at $R_{GC} \approx 18.5$ kpc.³⁵ Using age estimates from the MWSC catalog, our sample spans a range in age from ~ 5 Myr to ~ 6 Gyr,³⁶ with nearly half under 1 Gyr.

4.1. Modifications to the High-quality Sample

Beyond those clusters excluded from analysis based on our visual inspection of their PM-cleaned CMDs, we have further

³⁴ The full url is https://www.sdss.org/dr16/data_access/value-added-catalogs/?vac_id=open-cluster-chemical-abundances-and-mapping-catalog.

³⁵ We note that Dias et al. (2002) find Be 29 to be significantly further away at $R_{GC} \approx 22.5$ kpc, but for consistency, we are using distances from the MWSC catalog for all clusters.

³⁶ We note that some studies of NGC 6791 (e.g., Brogaard et al. 2012) find it to be significantly older; however, in the interest of a uniform analysis, we rely only on ages from the MWSC catalog.

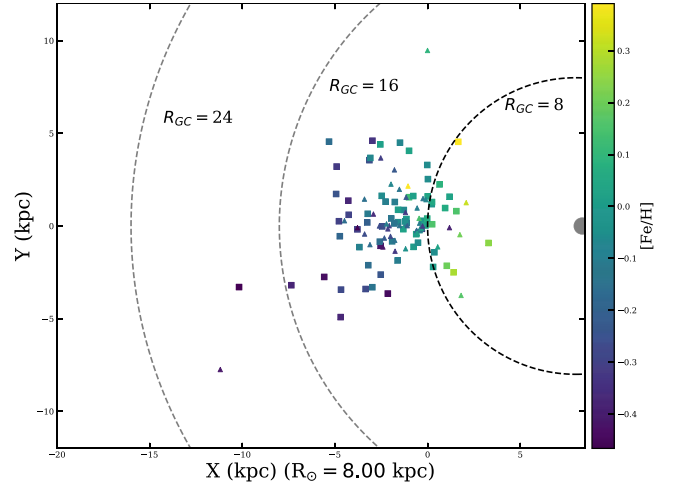


Figure 2. The full OCCAM DR16 sample plotted in the Galactic plane. Square points are “high-quality” clusters, triangles are the lower-quality clusters. The colorbar shows [Fe/H]. The concentric circles show $R_{GC} = 8, 16, \& 24$ kpc.

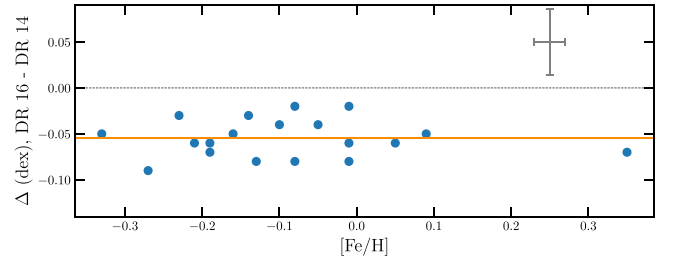


Figure 3. Difference in reported [Fe/H] from DR14 to DR16 for the 19 clusters from OCCAMII. Characteristic error bar is shown.

excluded 12 clusters (ASCC 16, ASCC 19, ASCC 21, Briceno 1, Chupina 1, Chupina 3, Collinder 69, Collinder 70, IC 348, NGC 1980, NGC 1981, and NGC 2264) because they are reported to be very young (< 50 Myr) (Kharchenko et al. 2013) and previous studies of young stars in APOGEE suggest the pipeline results may be unreliable (e.g., Kounkel et al. 2018). Thus, the final sample used for analysis consists of 71 clusters.

There are additional effects within clusters that may result in unreliable abundance determinations. Souto et al. (2018, 2019) showed that abundances in dwarf and giant stars in the old cluster NGC 2682 differed significantly due to atomic diffusion. For this reason, the dwarf stars in NGC 2682 are excluded from our abundance analysis. NGC 752 is also relatively old and may suffer from diffusion effects. Therefore, we exclude the dwarfs in this cluster from abundance analysis as well. As a result, for both NGC 752 and NGC 2682, we only use the giant stars to determine the cluster abundances.

4.2. Comparison to Previous Work

4.2.1. OCCAM PAPER II

For the 19 open clusters studied in OCCAMII, we plot Δ [Fe/H] versus DR16 [Fe/H] in Figure 3. Figure 3 shows that the mean [Fe/H] for OCCAM clusters changed between APOGEE DR14 and DR16; this is mostly due to changes in the gf values of the Fe I lines in the DR16 line list (V. V. Smith et al. 2020, in preparation). There is a clear offset for all clusters, with a mean difference of 0.05 dex. In OCCAMII, it was shown that APOGEE DR14 [Fe/H] values for six well-

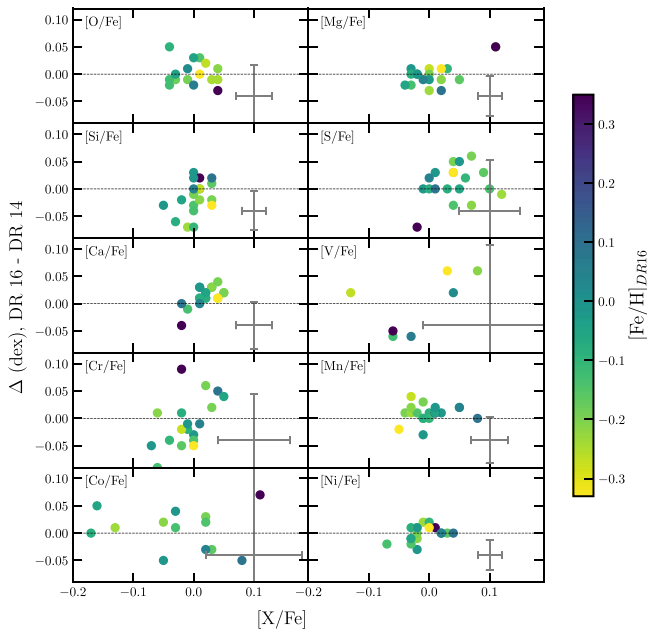


Figure 4. Similar to Figure 3, but for other elements. Characteristic error bars are shown. Data points are colored by their $[\text{Fe}/\text{H}]$, as reported in APOGEE DR16

studied open clusters were on average approximately 0.05 dex more metal-rich than the results in the literature. If we repeat the same literature comparison using our DR16 values, we find a mean offset of $[\text{Fe}/\text{H}] = 0.004$. All of these offsets are within their measured 1σ dispersions.

Figure 4 shows a similar plot for other elements. Beyond the quoted uncertainties in each case, there are no obvious systematic trends for any of these elements.

4.2.2. Open Clusters Observed by the LAMOST Survey

Zhang et al. (2019) published mean abundances for open clusters using results from the LAMOST survey (Luo et al. 2015). Our sample includes 22 open clusters in common with Zhang et al. (2019), and we find a median offset in $[\text{Fe}/\text{H}]$ (in the sense LAMOST—APOGEE) of -0.01 dex; however, we note some significant outliers. Figure 5 shows the difference in $[\text{Fe}/\text{H}]$ between Zhang et al. (2019) and this work ($[\text{Fe}/\text{H}]_{\text{LAMOST}} - [\text{Fe}/\text{H}]_{\text{APOGEE}}$). There is fairly good agreement near solar metallicity, but toward lower metallicities (as measured by APOGEE), there are some clusters with highly discrepant results. The three clusters with the most discrepant metallicities, $\gtrsim 0.2$ dex, are Czernik 23, ASCC 21, and NGC 2264 (in increasing order by their APOGEE $[\text{Fe}/\text{H}]$). The two clusters off by ~ 0.4 dex (Czernik 23 and NGC 2264) have only one star in the Zhang et al. (2019) analysis, and Czernik 23 has only one star in APOGEE as well. NGC 2264 and ASCC 21 are among the young clusters that were excluded from our high-quality sample. Removing these three most discrepant clusters, the LAMOST values are much more consistent with APOGEE.

A previous comparison of APOGEE DR14 to LAMOST found an offset in $[\text{Fe}/\text{H}]$ of 0.06 with a scatter of 0.13 (Anguiano et al. 2018). Given the analysis in Section 4.2.1, it is not surprising that APOGEE DR16 appears to be in better agreement with LAMOST.

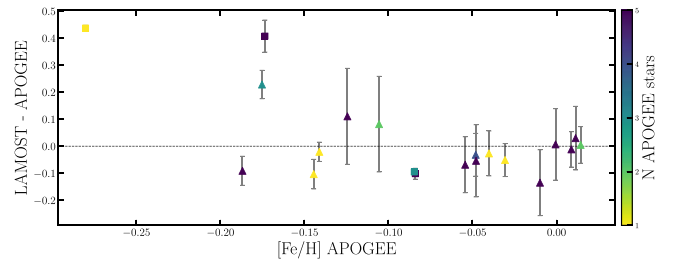


Figure 5. Difference between the metallicities in the LAMOST (from Zhang et al. 2019) and APOGEE surveys for open clusters in common. Color bar indicates the number of APOGEE stars in the cluster (saturating at 5). Square symbols denote clusters with a single star in Zhang et al. (2019).

5. Measuring Galactic Trends

5.1. Choosing a Distance Catalog

In OCCAMII, Galactocentric distances to open clusters were calculated using the average distance for member stars from Bailer-Jones et al. (2018). However, due to the application of a geometric prior to each star individually, this may not be an optimal solution for clusters (Bailer-Jones et al. 2018). Another uniform source of distances is therefore desired.

Distances to open clusters are frequently recomputed by many groups. Some form of isochrone fitting has been used by a number of studies (e.g., von Hippel et al. 2006; Kharchenko et al. 2013). However, only Kharchenko et al. (2013; MWSC) have produced a catalog using a uniform isochrone fitting method to measure distances for a very large (over 1000) set of open clusters. Recently, the *Gaia* survey has made it possible to create large catalogs of cluster distances based on parallax (e.g., Cantat-Gaudin et al. 2018). Of the two large catalogs, the MWSC catalog covers significantly more of our sample, but still, two clusters in our high-quality sample (BH 211 and Teutsch 12) are not included. For these clusters, we rely on stellar parallaxes from *Gaia* DR2. Since the MWSC catalog does not include distance uncertainties, we assume an uncertainty of 10% of the distance.

For completeness, and to highlight the significant influence that choosing a particular distance catalog can have on the measured gradient, Figure 6 repeats the basic analysis of Section 6 using three other distance catalogs (the catalogs of Dias et al. 2002 and Cantat-Gaudin et al. 2018, as well as inverse parallax as discussed in OCCAMII). The difference in the measured gradients is much less severe than in OCCAMII (where it was $\sim 40\%$), but it is still significant, potentially as large as $\sim 15\%$.

5.2. Fitting Galactic Abundance Gradients

It has become common in the literature, when measuring Galactic metallicity gradients, to divide the sample somewhere between $R_{\text{GC}} \approx 10$ kpc and $R_{\text{GC}} \approx 13$ kpc and fit two separate lines to the data (e.g., Twarog et al. 1997; Sestito et al. 2008; Friel et al. 2010; Carrera & Pancino 2011; Jacobson et al. 2011; Yong et al. 2012; Frinchaboy et al. 2013; Reddy et al. 2016; Magrini et al. 2017), with a much shallower trend in the outer galaxy than in the inner galaxy. Since the OCCAM sample includes open clusters as far away as $R_{\text{GC}} \approx 19$ kpc, we can investigate whether the Galactic metallicity gradient becomes significantly shallower at a given R_{GC} .

In this study, we fit two separate lines to the data and impose the additional constraint that both must meet at some “knee,”

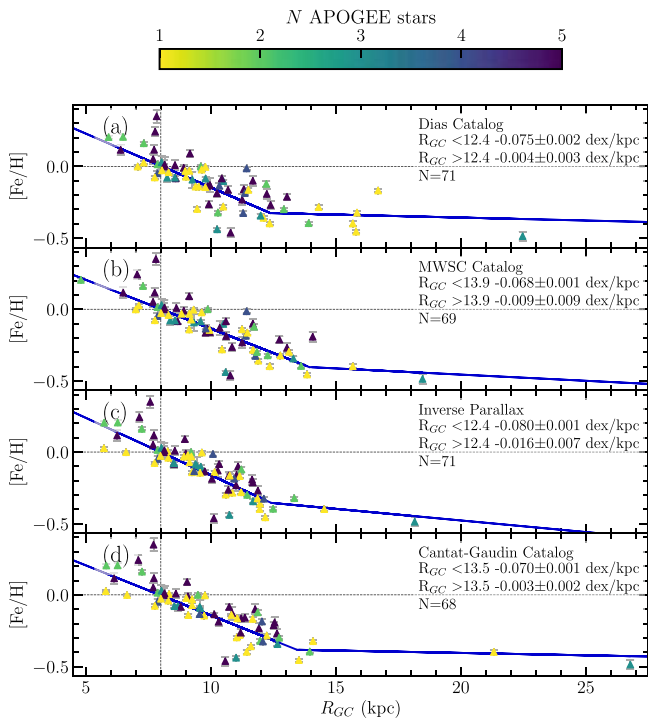


Figure 6. $[\text{Fe}/\text{H}]$ vs. R_{GC} trends measured using different distance determinations. This is similar to an analysis performed in OCCAMII, but we have added measurements from Cantat-Gaudin et al. (2018) where available. Color bar shows the number of APOGEE stars per cluster, saturating at 5.

although the location of the knee is allowed to vary. If we let k be the x -coordinate of the knee, the equation describing the fit line is then:

$$y = \begin{cases} m_1 \cdot x + b_1 & x \leq k \\ m_2 \cdot (x - k) + (m_1 \cdot k + b_1) & x > k \end{cases} \quad (1)$$

We estimate the values of m_1 , b_1 , m_2 , and k using maximum likelihood estimation. Uncertainties in each parameter are estimated using the *emcee* package (Foreman-Mackey et al. 2013). For trends that do not appear to have multiple components (e.g., $[\alpha/\text{Fe}]$ versus R_{GC} trends), we perform a maximum likelihood fit and *emcee* error estimation for a single line.

6. The Galactic Metallicity Gradient

Fitting to the overall $[\text{Fe}/\text{H}]$ versus R_{GC} gradient using open clusters as probes is common in many Galactic studies (e.g., Table 4 of OCCAMII). We fit the overall $[\text{Fe}/\text{H}]$ versus R_{GC} trend using our high-quality sample of 71 open clusters, with a two-line function fit (Figure 7). We find an inner ($R_{\text{GC}} < 13.9$ kpc) gradient of -0.068 ± 0.004 dex/kpc and an outer ($R_{\text{GC}} > 13.9$ kpc) gradient of -0.009 ± 0.011 dex/kpc.

A consensus on the apparent location of the “knee” has nearly been reached in the literature, with values converging around $R_{\text{GC}} \approx 12$ kpc. However, this location does not appear to have been rigorously tested; that is, the position of the “knee” has never been included as a free parameter in the fit.

We find the location of the break in the Galactic $[\text{Fe}/\text{H}]$ versus R_{GC} trend to be at $R_{\text{GC}} = 13.9$ kpc. To our knowledge, this is the first study to fit the “knee” as a free parameter. However, as shown in Figure 6, this is dependent on the

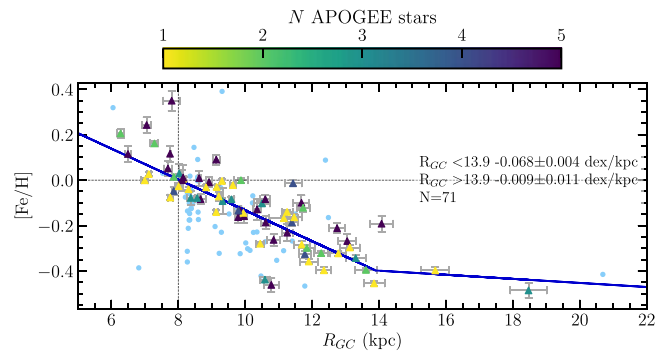


Figure 7. Full high-quality sample Galactic $[\text{Fe}/\text{H}]$ vs. R_{GC} trend, with a two-line fit (described by Equation (1)). Clusters flagged with quality “0” are shown as light blue circles. The color bar indicates the number of member stars per cluster, saturating at 5.

distance catalog adopted, and we recognize the poor coverage of our sample in the region $R_{\text{GC}} > 14$ kpc and the effect this may have on the determination of this parameter. Additional open clusters in this R_{GC} range have been targeted as part of APOGEE 2 and should be observed soon.

If we consider only the 19 open clusters studied in OCCAM II and fit a single line as in that previous study, we find a gradient of -0.047 ± 0.005 dex/kpc if we include NGC 6791 and -0.041 ± 0.005 dex/kpc if we do not include NGC 6791. OCCAM II found a gradient of -0.044 ± 0.003 dex/kpc using distances from the MWSC catalog and excluding NGC 6791. We emphasize that, although we find a global offset of 0.05 dex in $[\text{Fe}/\text{H}]$ between DR14 and DR16, this is not expected to have an effect on the slope of the $[\text{Fe}/\text{H}]$ versus R_{GC} trend, as the offset should be roughly similar at any given $[\text{Fe}/\text{H}]$. Given the comparison between gradients derived from DR14 and DR16 results, this appears to be the case.

Table 4 of OCCAMII summarized recent measurements of the Galactic metallicity gradient from the literature in the distance range considered of $6 \lesssim R_{\text{GC}} \lesssim 14$ kpc, and revealed a range of gradients between -0.052 dex/kpc to -0.085 dex/kpc. The result in this study of -0.068 dex/kpc sits neatly in the middle of this range.

We can compare in more detail to the recent results from Carrera et al. (2019), which also used APOGEE data (from DR14). The authors chose to split their sample at $R_{\text{GC}} = 11$ kpc, and find an inner gradient of -0.077 ± 0.007 dex/kpc. This is nearly in agreement with our result. We note that the authors used distances from Cantat-Gaudin et al. (2018); in Figure 6(d), we measure the metallicity gradient using the same distances and find a slope of -0.070 ± 0.001 dex/kpc, in good agreement with their result.

7. Galactic Trends for Other Elements

7.1. Galactic Trends for α -Elements

Figure 8 shows Galactic trends versus Fe for six α -elements (O, Mg, S, Si, Ca, and Ti). Because we find a break in the $[\text{Fe}/\text{H}]$ versus R_{GC} trend at $R_{\text{GC}} \approx 14$ kpc, we limit the sample to $R_{\text{GC}} < 14$ kpc and measure trends for the inner clusters. For all α elements studied here, except for silicon and titanium, there is a statistically significant slight positive trend from the inner galaxy to the outer galaxy, and the gradients in $[\alpha/\text{Fe}]$ are consistent overall. However, for silicon and titanium, we find a

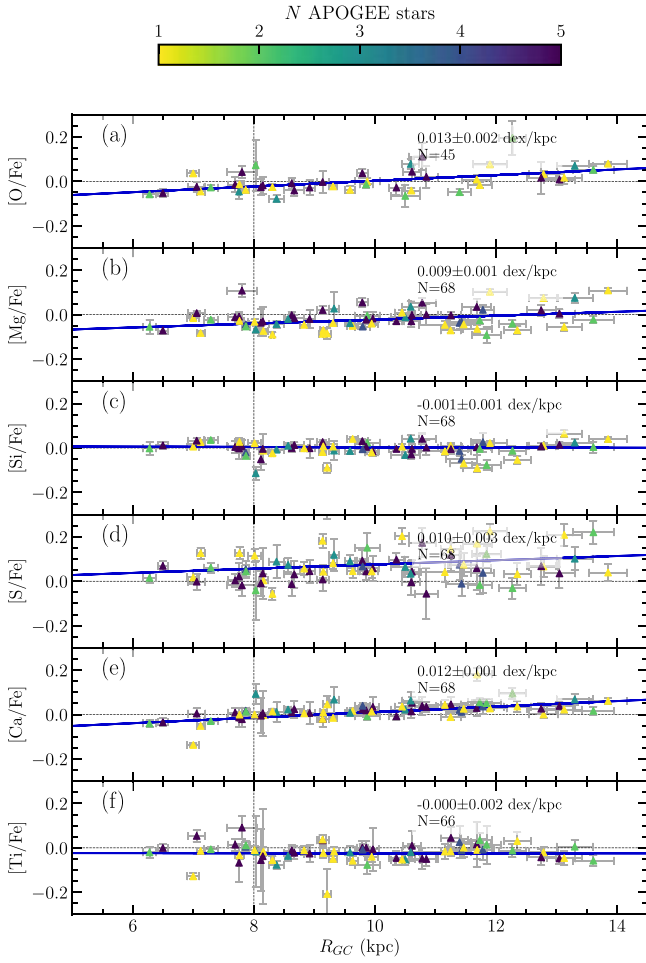


Figure 8. The $[X/Fe]$ vs. R_{GC} trend for α elements. As before, the color bar indicates number of member stars, saturating at 5.

flat gradient. We note there is significant scatter for $[S/Fe]$, and very little scatter for $[Ca/Fe]$.

Our results are consistent with Yong et al. (2012), who measured mild positive gradients for $[O/Fe]$, $[Si/Fe]$, and $[Ca/Fe]$, of the order of $0.01 \text{ dex kpc}^{-1}$, but a flat trend for $[Mg/Fe]$, although the uncertainties on all four trends are nearly as large as their measured gradients. Casamiquela et al. (2019) report slight positive gradients for $[Si/Fe]$ (0.022 ± 0.007) and $[Mg/Fe]$ (0.011 ± 0.01) in their uniform sample of open clusters in the range $6 \leq R_{GC} \leq 11 \text{ kpc}$, although both slopes are much shallower when they include more clusters from the literature. Carrera & Pancino (2011) and Reddy et al. (2016) report $[\alpha/Fe]$ versus R_{GC} gradients of $0.004 \pm 0.001 \text{ dex kpc}^{-1}$ and $0.014 \pm 0.005 \text{ dex kpc}^{-1}$, respectively. Our results are therefore in good agreement with the literature—except perhaps for Si, which appears to be almost completely flat in our case.

Recent work using APOGEE data showed a possible temperature effect for silicon abundances (Zasowski et al. 2019): cooler stars show lower abundances than warmer ones. The stars in more distant clusters tend to be cooler, since only brighter, more evolved stars are detectable farther away. Thus, the flat $[Si/Fe]$ trend may partly reflect this effect in APOGEE data.

7.2. Galactic Trends for Iron-peak Elements

APOGEE DR16 reports abundances for six elements that are classified as “iron-peak” elements: vanadium, chromium,

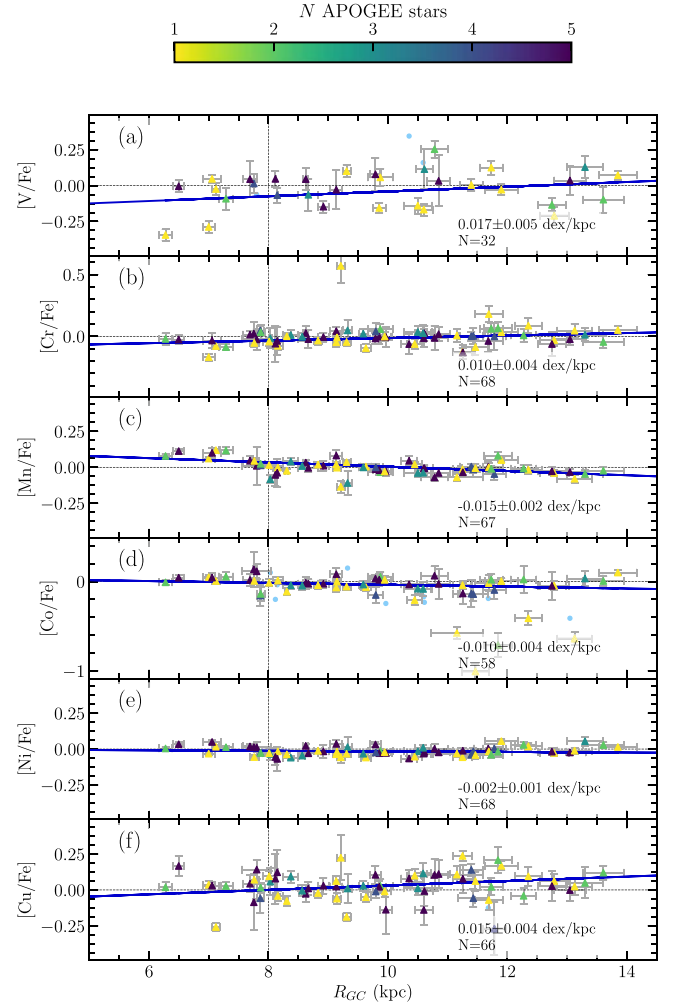


Figure 9. The $[X/Fe]$ vs. R_{GC} trend for iron-peak elements. Light blue circles are clusters that have an $[X/Fe]$ abundance reported but $\sigma [X/Fe] \geq 0.2 \text{ dex}$.

manganese, cobalt, nickel, and copper. Figure 9 shows Galactic abundance trends for each of these elements. The $[Ni/Fe]$ versus R_{GC} trend is completely flat; the abundances stay very near solar with small scatter for the Galactic radii explored. Statistically significant, slightly positive trends are measured for $[V/Fe]$, $[Cr/Fe]$, and $[Cu/Fe]$, but there are some significant outliers for $[Cr/Fe]$ (Czernik 18 having a single star with $[Cr/Fe] = +0.57$) and $[Cu/Fe]$ (Chupina 1 having a single star with $[Cu/Fe] = -0.58$). There is a statistically significant, slightly negative trend measured for $[Co/Fe]$, but a number of outliers to this trend are present between $R_{GC} \approx 11 \text{ kpc}$ and $R_{GC} \approx 13 \text{ kpc}$. Interestingly, Casamiquela et al. (2019) find a mildly significant *negative* trend for $[V/Fe]$. For $[Cr/Fe]$, they find conflicting trends depending on which sample they use. This suggests a need for more observational data to better constrain the gradients in these elements.

For $[Mn/Fe]$, a significant negative trend of -0.015 ± 0.002 is found. We note that this is consistent with the trend first presented in OCCAMII. Yong et al. (2012) find a $[Mn/Fe]$ gradient of -0.06 ± 0.01 in the region $R_{GC} < 13 \text{ kpc}$, but this measurement is made using only ~ 8 open clusters. Since this trend is not well-studied, little discussion of it exists in the literature. A relatively simple explanation may be that higher $[Mn/Fe]$ abundances in the inner Galaxy are the result of larger contributions to chemical enrichment from type Ia supernovae (SNe Ia) (Nomoto et al. 2013),

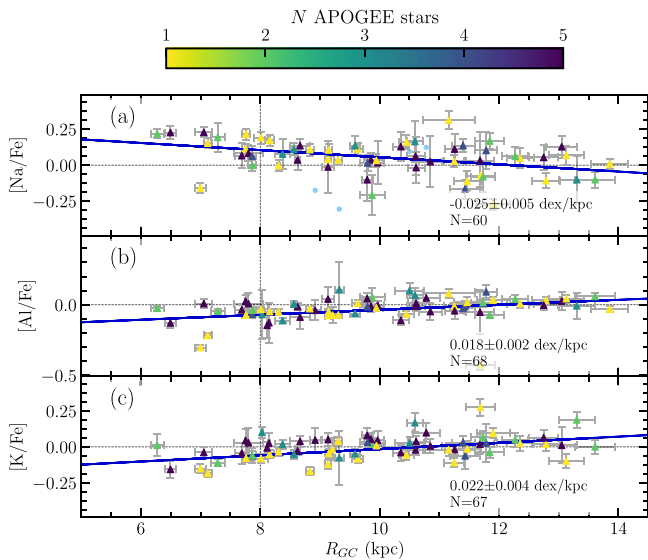


Figure 10. The $[X/Fe]$ vs. R_{GC} trend for the “odd- z ” elements reported in APOGEE DR16. As before, the color bar indicates number of members, and light blue circles are clusters with very high uncertainty in that element.

perhaps suggesting less recent star formation toward the inner galaxy or higher SNe Ia efficiency in the inner Galaxy.

7.3. “Odd- z ” Gradients

There are three other APOGEE elements that do not readily fall into the above categories: sodium, aluminum, and potassium, often referred to as “odd- z ” elements. We note that while $[P/Fe]$ abundances are reported in DR16, there are serious doubts about the reliability of the abundances for this element (see H. Jönsson et al. 2020, in preparation). Figure 10 shows the Galactic trends for $[Na/Fe]$, $[Al/Fe]$, and $[K/Fe]$. $[Al/Fe]$ and $[K/Fe]$ show nearly identical significant positive gradients, while $[Na/Fe]$ shows a significant negative gradient. All three trends have at least one significant outlier, but the trends nevertheless appear fairly robust. Yong et al. (2012) find a similar trend for $[Al/Fe]$ of 0.03 ± 0.01 dex/kpc; for $[Na/Fe]$, however, they find a flat trend with significant scatter.

8. The Evolution of Galactic Abundance Gradients

Minchev et al. (2019) discuss the effect that sample selection can have on measured abundance gradients, in particular the bias introduced by most samples containing a majority of young clusters. To more accurately compare to previous work, and to provide more meaningful comparisons for galactic evolution models, in this section we compare mono-age samples.

8.1. Iron

Our sample is large enough that it can be split into four age bins, which we divide at 400 Myr, 800 Myr, and 2 Gyr, with all bins being reasonably well populated. Figure 11 shows the $[Fe/H]$ versus R_{GC} trend for clusters separated in age bins. We use ages from the MWSC catalog because they are derived in a uniform fashion, and should certainly be reliable enough to place clusters in the coarse bins we have chosen.

The evolution of the $[Fe/H]$ versus R_{GC} trend has been studied extensively in the literature (e.g., Carraro et al. 1998; Friel et al. 2002; Carrera & Pancino 2011; Jacobson et al. 2011;

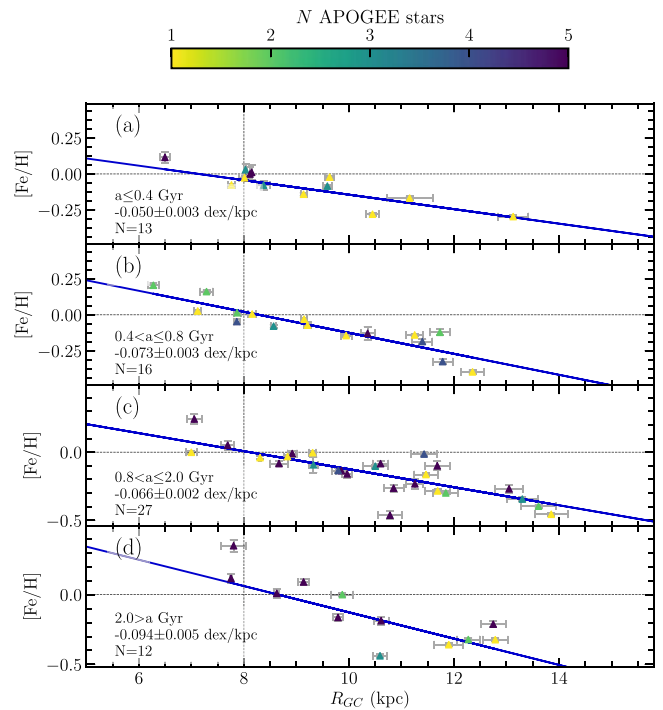


Figure 11. Galactic $[Fe/H]$ vs. R_{GC} trend in four age bins, showing the general decrease in steepness over time.

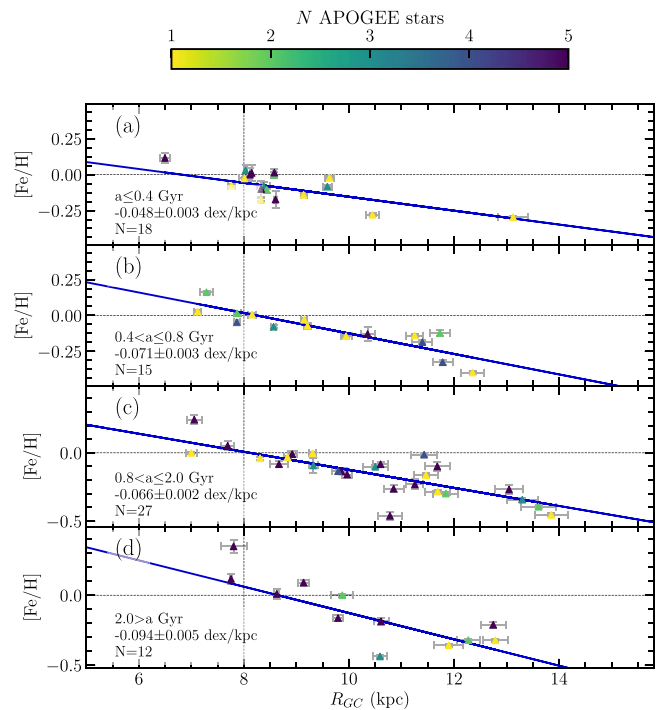


Figure 12. Summary of Galactic metallicity gradients measured in mono-age populations from the literature.

Yong et al. 2012). A summary of results from the literature is provided in Figure 12. Here, we plot the measured metallicity gradient for clusters in a given age range versus the middle of that age range (for example the middles of our age bins are 0.2, 0.6, 1.4, 4 Gyr). It is important to note that the majority of clusters from all four studies in Figure 12 fall in the range $R_{GC} < 14$ kpc, with the exception of a few clusters from Carraro et al. (1998). Figure 12 shows a consistent trend of

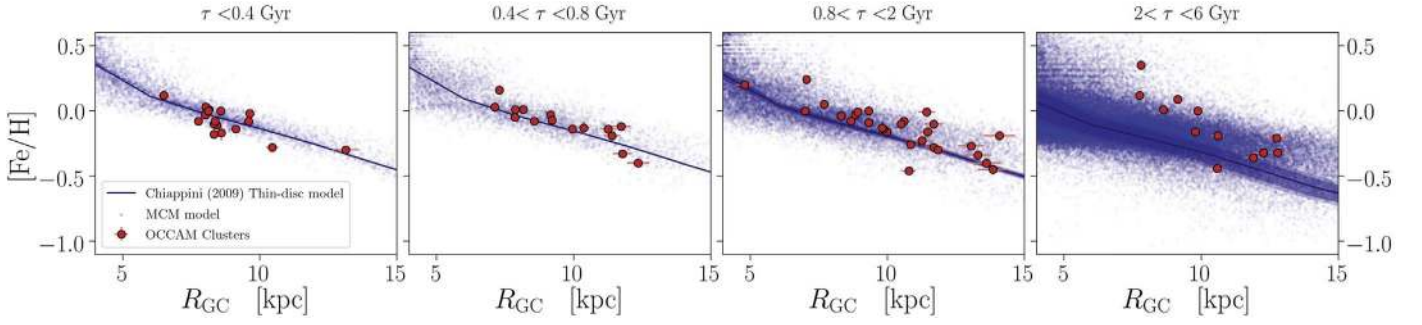


Figure 13. OCCAM IV clusters (red) plotted with the pure chemical evolution model of Chiappini (2009) (blue line) and the MCM chemo-dynamical simulation (Minchev et al. 2013, 2014), separated into the age bins used previously.

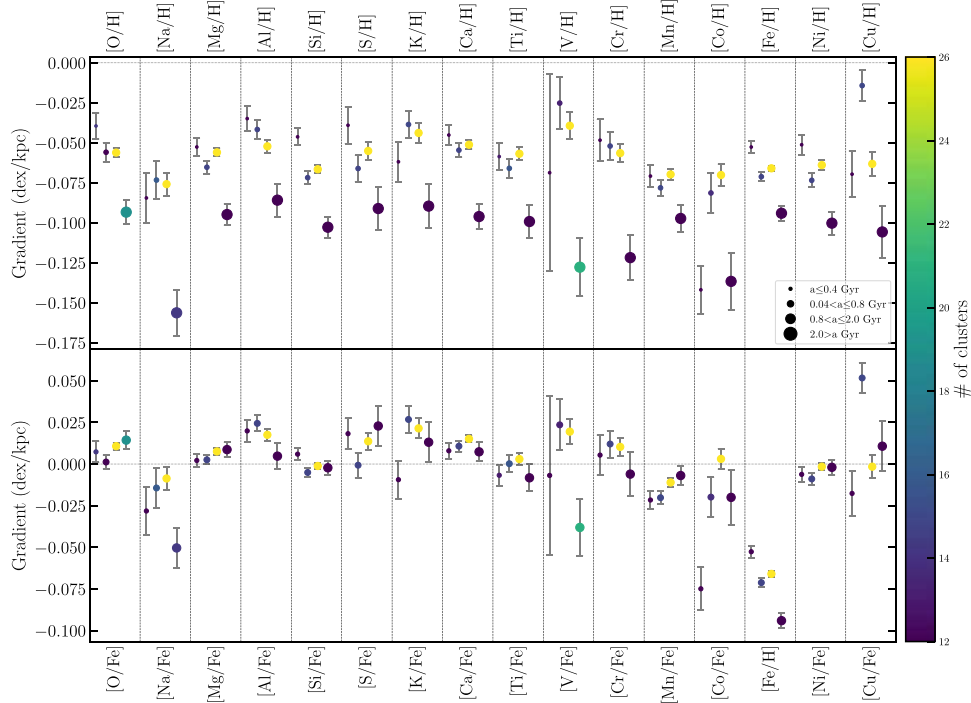


Figure 14. Gradients measured in four age bins as for Figure 11 are plotted for each element. Points increase in size from youngest to oldest; the color indicates number of clusters used to measure each gradient.

steeper metallicity gradients for older populations. There is one point in disagreement with this trend: the oldest clusters from Carraro et al. (1998) appear to reverse this trend. This may be due to the inclusion of some clusters near $R_{GC} \approx 15$ in their oldest bin. If we consider the large uncertainties on the two oldest measurements, it is possible the trend levels out after 4 Gyr.

It should be mentioned that the trend found here is opposite that seen for field stars (e.g., Anders et al. 2017), where the oldest populations show a shallower gradient. Radial migration is expected to cause this flattening of the metallicity gradient on a long enough timescale (e.g., Minchev et al. 2018). To explain the absence of this phenomenon in open clusters, Anders et al. (2017) suggest that clusters that do not migrate or clusters that migrate toward the inner Galaxy preferentially break up.

In Figure 13, we show the OCCAM IV sample plotted with the pure chemical evolution model of Chiappini (2009) and the chemo-dynamical simulation of Minchev et al. (2013, 2014; MCM), divided in the same age bins as Figure 11. There is good agreement between the models and the OCCAM IV

sample in the younger three bins. In the oldest bin, the effects of radial migration are clearly seen in the MCM points. Also in the oldest bin, there is a noticeable lack of clusters toward the inner galaxy, as well as a clear steepening of the gradient, which could be due to migration of inner old clusters toward outer regions. This is consistent with the suggestion from Anders et al. (2017) that clusters migrating inward preferentially break up. Elsewhere, the clusters are roughly consistent with the MCM model.

8.2. Other Elements

Age trends in elements other than iron also provide insight into the chemical evolution of the Galaxy. The top panel of Figure 14 provides a summary of abundance gradients for each element presented previously as a function of cluster age, measured in the same four age bins as for iron (Figure 11). The top panel of Figure 14 shows an overall similar behavior for all elements: the gradient for the oldest population (open clusters older than ~ 2 Gyr) is the steepest; this is reminiscent of what was observed for [Fe/H]. For [Na/H], [Ti/H], [Cr/H], and

[Mn/H], we cannot distinguish between the gradients measured for the intermediate-age and young populations. For [O/H], [Mg/H], [Si/H], [S/H], [K/H], [V/H], [Co/H], [Fe/H], and [Ni/H], the youngest population shows a distinctly flatter gradient, but the two intermediate-age populations are indistinguishable within the uncertainties. Relatively flat α -element abundance gradients have also been found for young B stars (e.g., Daflon & Cunha 2004) and H II regions (e.g., Esteban et al. 2015). We note that, for [V/H], the youngest bin is populated with only five clusters, while for [Co/H], the gradient in the youngest population is heavily influenced by a single very [Co/H]-poor cluster.

8.3. The Evolution of $[X/Fe]$ Gradients

To understand the differences in the evolution of elemental abundances better, it is also informative to study the evolution of $[X/Fe]$ gradients over time. The bottom panel of Figure 14 is similar to the top panel, but now we show the evolution of $[X/Fe]$ trends. A variety of trends can be seen; some elements show a stable trend over time (e.g., [Ni/Fe], [Si/Fe]), some show an increasingly positive trend (e.g., [Al/Fe]), and [Mn/Fe] shows an increasingly negative trend. All of these trends are worth discussing, and we do so below. We do not consider [V/Fe], [Cr/Fe], [Co/Fe], or [Cu/Fe] in detail, either because the uncertainties are larger than the trends or because one or more age bins are poorly populated for that element. We do not discuss [Ni/Fe] further because, as stated in Section 7.2, Ni appears to track Fe closely.

The results in Figure 14 show no clear evidence of evolution in the $[\alpha/Fe]$ gradients within the time spanned by this open cluster sample. It could be argued that there are mild trends with age for the [O/Fe], [Mg/Fe], and [Ca/Fe] gradients, but the changes between different aged populations are on the order of the uncertainties. For [Si/Fe], [S/Fe], and [Ti/Fe], there are more variations, but also larger uncertainties and it is more appropriate to consider the gradients as roughly constant for different aged populations. It was shown in Figure 8 that nearly all of the $[\alpha/Fe]$ abundances exhibit mildly increasing radial trends, and Figure 14 indicates that such trends appear to be fairly stable within the time spanned by our cluster sample. The flattening of the abundance gradients in recent times suggests more recent chemical enrichment in the outer Galaxy, but taken together with the stability of the increasing $[\alpha/Fe]$ gradient, we might deduce that the enrichment in the outer Galaxy had a more significant contribution from core-collapse supernovae. This is consistent with the conclusions from Section 7.2 and the discussion below, that supernovae Ia dominated recent enrichment in the inner Galaxy.

For [Na/Fe] and [Al/Fe], the gradients for the oldest clusters are clearly set apart, even considering the sizeable uncertainty. For [Al/Fe], in particular, there appears to be a clear trend where we see the younger populations showing an increasingly positive slope. Significantly larger Na and Al yields are expected from core-collapse supernovae than SNe Ia (Nomoto et al. 2013), so a flattening of the [Na/Fe] gradient and an increasingly positive [Al/Fe] gradient are both consistent with either more recent star formation in the outer Galaxy than the inner Galaxy or higher SNe Ia efficiency in the inner Galaxy. This is also consistent with the explanation for the [Mn/Fe] gradient in Section 7.2.

Figure 14 shows that the [Mn/Fe] gradient becomes more negative for younger cluster populations. Yamaguchi et al. (2015)

showed that SNe Ia yields of manganese are strongly dependent on progenitor metallicity; higher-metallicity progenitors will yield significantly more manganese. So, as metals build up in the inner Galaxy, a higher [Mn/Fe] abundance is expected. This may explain the evolution of the [Mn/Fe] gradient in general terms.

9. Conclusions

We present a sample of 128 open clusters, 71 of which we designate as “high quality,” using APOGEE DR16. We demonstrate that DR16 cluster abundances are in good agreement with those of other high-resolution abundance studies. Using the high-quality sample, we measure Galactic abundance gradients in 16 chemical elements, and we measure how those gradients change for different age samples.

We find an overall Galactic [Fe/H] versus R_{GC} gradient of -0.068 ± 0.004 dex kpc^{-1} for $R_{GC} < 13.9$ kpc, but we re-emphasize the point of OCCAMII that this result can vary significantly depending on which catalog of distances is used. We show general agreement with the literature in regards to the evolution of this gradient.

For the first time, we fit the knee in the Galactic abundance gradient as a free parameter at $R_{GC} = 13.9$ kpc, but we recognize a need for more clusters beyond this break to more reliably constrain the fit.

We find general agreement with the literature for gradients in α elements. We present further evidence for the negative [Mn/Fe] versus R_{GC} trend first found in OCCAMII. We find significant Galactic trends in vanadium, chromium, and copper, although we are unable to suggest a strong explanation for these trends. We find very significant trends in sodium, aluminum, and potassium; so-called “odd-Z” elements. We recognize a need for further study of trends in these elements, as they are not well-reported in the literature.

We divide our sample into four age bins and investigate changes in 16 elements over time. We show that $[X/H]$ abundance gradients for all 16 elements follow the same general trend, becoming more shallow over time, as has consistently been found for iron. We further investigate age trends in $[X/Fe]$ for 15 elements. A number of these trends seem to support a similar conclusion: either increased SNe Ia efficiency toward the inner Galaxy or less recent star formation in the inner Galaxy compared to the outer Galaxy.

We would like to thank Marina Kounkel for very helpful discussions about young clusters. We would also like to thank José G. Fernández-Trincado and Borja Anguiano for helpful comments.

J.D. and P.M.F. acknowledge support for this research from the National Science Foundation (AST-1311835 & AST-1715662). K.C. acknowledges support for this research from the National Science Foundation (AST-0907873).

D.A.G.H. acknowledges support from the State Research Agency (AEI) of the Spanish Ministry of Science, Innovation, and Universities (MCIU), and the European Regional Development Fund (FEDER) under grant AYA2017-88254-P.

D.G. and D.M. gratefully acknowledge support from the Chilean Centro de Excelencia en Astrofísica y Tecnologías Afines (CATA) BASAL grant AFB-170002. D.G. also acknowledges financial support from the Dirección de Investigación y Desarrollo de la Universidad de La Serena through the Programa de Incentivo a la Investigación de Académicos (PIA-DIDULS). D.M. is also supported by the Programa Iniciativa Científica Milenio

grant IC120009, awarded to the Millennium Institute of Astrophysics (MAS), and by Proyecto FONDECYT regular No. 1170121.

H.J. acknowledges support from the Crafoord Foundation, Stiftelsen Olle Engkvist Byggmästare, and Ruth och Nils-Erik Stenbäck's stiftelse.

A.R.-L. acknowledges financial support provided in Chile by Comisión Nacional de Investigación Científica y Tecnológica (CONICYT) through the FONDECYT project 1170476 and by the QUIMAL project 130001

Funding for SDSS-III has been provided by the Alfred P. Sloan Foundation, the Participating Institutions, the National Science Foundation, and the U.S. Department of Energy Office of Science. The SDSS-III website is <http://www.sdss3.org/>.

SDSS-III is managed by the Astrophysical Research Consortium for the Participating Institutions of the SDSS-III Collaboration including the University of Arizona, the Brazilian Participation Group, Brookhaven National Laboratory, Carnegie Mellon University, University of Florida, the French Participation Group, the German Participation Group, Harvard University, the Instituto de Astrofísica de Canarias, the Michigan State/Notre Dame/JINA Participation Group, Johns Hopkins University, Lawrence Berkeley National Laboratory, Max Planck Institute for Astrophysics, Max Planck Institute for Extraterrestrial Physics, New Mexico State University, New York University, Ohio State University, Pennsylvania State University, University of Portsmouth, Princeton University, the Spanish Participation Group, University of Tokyo, University of Utah, Vanderbilt University, University of Virginia, University of Washington, and Yale University.

Funding for the Sloan Digital Sky Survey IV has been provided by the Alfred P. Sloan Foundation, the U.S. Department of Energy Office of Science, and the Participating Institutions. SDSS-IV acknowledges support and resources from the Center for High-Performance Computing at the University of Utah. The SDSS website is www.sdss.org.

SDSS-IV is managed by the Astrophysical Research Consortium for the Participating Institutions of the SDSS Collaboration including the Brazilian Participation Group, the Carnegie Institution for Science, Carnegie Mellon University, the Chilean Participation Group, the French Participation Group, Harvard-Smithsonian Center for Astrophysics, Instituto de Astrofísica de Canarias, The Johns Hopkins University, Kavli Institute for the Physics and Mathematics of the Universe (IPMU)/University of Tokyo, Lawrence Berkeley National Laboratory, Leibniz Institut für Astrophysik Potsdam (AIP), Max-Planck-Institut für Astronomie (MPIA Heidelberg), Max-Planck-Institut für Astrophysik (MPA Garching), Max-Planck-Institut für Extraterrestrische Physik (MPE), National Astronomical Observatories of China, New Mexico State University, New York University, University of Notre Dame, Observatório Nacional/MCTI, The Ohio State University, Pennsylvania State University, Shanghai Astronomical Observatory, United Kingdom Participation Group, Universidad Nacional Autónoma de México, University of Arizona, University of Colorado Boulder, University of Oxford, University of Portsmouth, University of Utah, University of Virginia, University of Washington, University of Wisconsin, Vanderbilt University, and Yale University.

This work has made use of data from the European Space Agency (ESA) mission *Gaia* (<https://www.cosmos.esa.int/gaia>), processed by the *Gaia* Data Processing and Analysis

Consortium (DPAC, <https://www.cosmos.esa.int/web/gaia/dpac/consortium>). Funding for the DPAC has been provided by national institutions, in particular the institutions participating in the *Gaia* Multilateral Agreement.

This research made use of Astropy, a community-developed core Python package for Astronomy (Astropy Collaboration, 2018).

Facilities: Sloan (APOGEE), FLWO:2MASS, *Gaia*.

Software: Astropy.³⁷

ORCID iDs

Peter M. Frinchaboy  <https://orcid.org/0000-0002-0740-8346>

Katia Cunha  <https://orcid.org/0000-0001-6476-0576>

Rachael Beaton  <https://orcid.org/0000-0002-1691-8217>

Dmitry Bizyaev  <https://orcid.org/0000-0002-3601-133X>

Joel R. Brownstein  <https://orcid.org/0000-0002-8725-1069>

Ricardo Carrera  <https://orcid.org/0000-0001-6143-8151>

Doug Geisler  <https://orcid.org/0000-0002-3900-8208>

Dante Minniti  <https://orcid.org/0000-0002-7064-099X>

Kaike Pan  <https://orcid.org/0000-0002-2835-2556>

Alexandre Roman-Lopes  <https://orcid.org/0000-0002-1379-4204>

Gail Zasowski  <https://orcid.org/0000-0001-6761-9359>

References

- Ahumada, R., Allende Prieto, C., Almeida, A., et al. 2019, arXiv:1912.02905
- Anders, F., Chiappini, C., Minchev, I., et al. 2017, *A&A*, **600**, A70
- Anguiano, B., Majewski, S. R., Allende-Prieto, C., et al. 2018, *A&A*, **620**, A76
- Bailer-Jones, C. A. L., Rybizki, J., Fouesneau, M., Mantelet, G., & Andrae, R. 2018, *AJ*, **156**, 58
- Blanton, M. R., Bershad, M. A., Abolfathi, B., et al. 2017, *AJ*, **154**, 28
- Bowen, I. S., & Vaughan, A. H. J. 1973, *ApOpt*, **12**, 1430
- Bragaglia, A., Sestito, P., Villanova, S., et al. 2008, *A&A*, **480**, 79
- Brogaard, K., Vandenberg, D. A., Bruntt, H., et al. 2012, *A&A*, **543**, A106
- Burger, D., Stassun, K. G., Pepper, J., et al. 2013, *A&C*, **2**, 40
- Cantat-Gaudin, T., Jordi, C., Vallenari, A., et al. 2018, *A&A*, **618**, A93
- Carrera, G., Ng, Y. K., & Portinari, L. 1998, *MNRAS*, **296**, 1045
- Carrera, R., Bragaglia, A., Cantat-Gaudin, T., et al. 2019, *A&A*, **623**, A80
- Carrera, R., & Pancino, E. 2011, *A&A*, **535**, A30
- Casamiquela, L., Blanco-Cuaresma, S., Carrera, R., et al. 2019, *MNRAS*, **490**, 1821
- Chiappini, C. 2009, in IAU Symp. 254, The Galaxy Disk in Cosmological Context, ed. J. Andersen, B. Nordström, & J. Bland-Hawthorn (Cambridge: Cambridge Univ. Press), 191
- Cunha, K., Frinchaboy, P. M., Souto, D., et al. 2016, *AN*, **337**, 922
- Cunha, K., Smith, V. V., Hasselquist, S., et al. 2017, *ApJ*, **844**, 145
- Dafon, S., & Cunha, K. 2004, *ApJ*, **617**, 1115
- Dias, W. S., Alessi, B. S., Moitinho, A., & Lépine, J. R. D. 2002, *A&A*, **389**, 871
- Donor, J., Frinchaboy, P. M., Cunha, K., et al. 2018, *AJ*, **156**, 142
- Esteban, C., García-Rojas, J., & Pérez-Mesa, V. 2015, *MNRAS*, **452**, 1553
- Foreman-Mackey, D., Hogg, D. W., Lang, D., & Goodman, J. 2013, *PASP*, **125**, 306
- Friel, E. D., Jacobson, H. R., & Pilachowski, C. A. 2010, *AJ*, **139**, 1942
- Friel, E. D., Janes, K. A., Tavares, M., et al. 2002, *AJ*, **124**, 2693
- Frinchaboy, P. M., Thompson, B., Jackson, K. M., et al. 2013, *ApJL*, **777**, L1
- Gaia Collaboration, Brown, A. G. A., Vallenari, A., et al. 2018, *A&A*, **616**, A1
- Gaia Collaboration, Prusti, T., de Bruijne, J. H. J., et al. 2016, *A&A*, **595**, A1
- García Pérez, A. E., Allende Prieto, C., Holtzman, J. A., et al. 2016, *AJ*, **151**, 144
- Gunn, J. E., Sigmund, W. A., Mannery, E. J., et al. 2006, *AJ*, **131**, 2332
- Hasselquist, S., Shetrone, M., Cunha, K., et al. 2016, *ApJ*, **833**, 81
- Holtzman, J. A., Hasselquist, S., Shetrone, M., et al. 2018, *AJ*, **156**, 125
- Holtzman, J. A., Shetrone, M., Johnson, J. A., et al. 2015, *AJ*, **150**, 148
- Jacobson, H. R., Friel, E. D., Jilková, L., et al. 2016, *A&A*, **591**, A37
- Jacobson, H. R., Pilachowski, C. A., & Friel, E. D. 2011, *AJ*, **142**, 59

³⁷ <http://www.astropy.org/>

- Janes, K. A. 1979, *ApJS*, 39, 135
- Kharchenko, N. V., Piskunov, A. E., Schilbach, E., Röser, S., & Scholz, R.-D. 2013, *A&A*, 558, A53
- Kounkel, M., Covey, K., Suárez, G., et al. 2018, *AJ*, 156, 84
- Lindegren, L., Hernandez, J., Bombrun, A., et al. 2018, *A&A*, 616, A2
- Luo, A. L., Zhao, Y.-H., Zhao, G., et al. 2015, *RAA*, 15, 1095
- Magrini, L., Randich, S., Kordopatis, G., et al. 2017, *A&A*, 603, A2
- Majewski, S. R., Schiavon, R. P., Frinchaboy, P. M., et al. 2017, *AJ*, 154, 94
- Mészáros, S., Allende Prieto, C., Edvardsson, B., et al. 2012, *AJ*, 144, 120
- Minchev, I., Anders, F., Recio-Blanco, A., et al. 2018, *MNRAS*, 481, 1645
- Minchev, I., Chiappini, C., & Martig, M. 2013, *A&A*, 558, A9
- Minchev, I., Chiappini, C., & Martig, M. 2014, *A&A*, 572, A92
- Minchev, I., Matijevic, G., Hogg, D. W., et al. 2019, *MNRAS*, 487, 3946
- Nidever, D. L., Holtzman, J. A., Allende Prieto, C., et al. 2015, *AJ*, 150, 173
- Nomoto, K., Kobayashi, C., & Tominaga, N. 2013, *ARA&A*, 51, 457
- Reddy, A. B. S., Lambert, D. L., & Giridhar, S. 2016, *MNRAS*, 463, 4366
- Sestito, P., Bragaglia, A., Randich, S., et al. 2008, *A&A*, 488, 943
- Skrutskie, M. F., Cutri, R. M., Stiening, R., et al. 2006, *AJ*, 131, 1163
- Souto, D., Allende Prieto, C., Cunha, K., et al. 2019, *ApJ*, 874, 97
- Souto, D., Cunha, K., Smith, V. V., et al. 2018, *ApJ*, 857, 14
- Twarog, B. A., Ashman, K. M., & Anthony-Twarog, B. J. 1997, *AJ*, 114, 2556
- von Hippel, T., Jefferys, W. H., Scott, J., et al. 2006, *ApJ*, 645, 1436
- Wilson, J. C., Hearty, F. R., Skrutskie, M. F., et al. 2019, *PASP*, 131, 055001
- Wright, E. L., Eisenhardt, P. R. M., Mainzer, A. K., et al. 2010, *AJ*, 140, 1868
- Yamaguchi, H., Badenes, C., Foster, A. R., et al. 2015, *ApJL*, 801, L31
- Yong, D., Carney, B. W., & Friel, E. D. 2012, *AJ*, 144, 95
- Yong, D., Carney, B. W., & Teixeira de Almeida, M. L. 2005, *AJ*, 130, 597
- Zamora, O., García-Hernández, D. A., Allende Prieto, C., et al. 2015, *AJ*, 149, 181
- Zasowski, G., Cohen, R. E., Chojnowski, S. D., et al. 2017, *AJ*, 154, 198
- Zasowski, G., Johnson, J. A., Frinchaboy, P. M., et al. 2013, *AJ*, 146, 81
- Zasowski, G., Schultheis, M., Hasselquist, S., et al. 2019, *ApJ*, 870, 138
- Zhang, J., Zhao, J., Oswalt, T. D., et al. 2019, *ApJ*, 887, 84